Proceedings of the
Annual Stability Conference
Structural Stability Research Council
Toronto, Canada, March 25-28, 2014

Lateral bracing requirements for H-section beams with supports attached to top flange subjected to cyclic antisymmetric moment

R. Matsui[1], Y. Yamaura[2], T. Takeuchi[3]

Abstract

Lateral-torsional buckling is one of the key factors determining the ductile behavior of steel moment frames. The current lateral bracing requirements for beams have been established based on monotonic loading conditions in current seismic provisions. However, the relationship between the current provisions and the required lateral bracing stiffness under cyclic loading has not yet been systematically confirmed. In this study, an experiment was conducted to assess the effect of the lateral support stiffness on the strength of the H-section beam, under cyclic loading. Three different types of lateral supports were examined under cyclic antisymmetric moment. Numerical analysis was used to simulate the experimental results and compute the effects of the lateral support stiffness, unbraced length, sectional stiffener mount, and dead load condition on the H-section beam's elastoplastic lateral-torsional buckling behavior. The results are compared to the requirements in the current provisions and discussed in this paper.

1. Introduction

Lateral-torsional buckling is one of the key factors determining the ductile behavior of steel moment frames. Assessing lateral support requirements is important for preventing strength degradation in the beams during elastoplastic design. Many researchers (Galambos (1963), Wakabayashi et al. (1983)) have conducted experiments and numerical simulations of the elastoplastic lateral buckling behavior of H-section beams under monotonic loading, and the current provisions are specified by the results of those studies. However, the same behavior under cyclic loading has not been clarified yet.

Nakashima et al. (2002) conducted experiments of the beam-column frame and reported that elastoplastic lateral buckling strength degrades under cyclic loading compared to that under monotonic loading. Additionally, using a function of moment gradient, the requirement for unbraced length is proposed to maintain adequate deformation capacity. Liu et al. (2003) conducted experiments and numerical simulations of the complete failure behavior of H-section beams subjected to cyclic loading, and proposed the condition for unbraced length and width-thickness ratio.

In these investigations, lateral supports were attached to both top and bottom flanges. However, those regularly used in practical design are either continuous (by embedding only the top flange

[1] Assistant Professor, Tokyo Institute of Technology, <matsui.r.aa@m.titech.ac.jp>
[2] Structural Engineer, Yamashita Sekkei Inc., <yamaura-y@yamashitasekkei.co.jp>
[3] Professor, Tokyo Institute of Technology, <ttoru@arch.titech.ac.jp>

in a concrete slab) or attached to only the top flange. For these types, the Recommendation for Limit State Design (LSD) of Steel Structures of the Architectural Institute of Japan (AIJ) provides beam bracing requirements, as summarized in Section 2. Ando and Ono (2005) conducted numerical simulations and indicated that additional investigation of the stiffness and strength of lateral supports is required for meeting LSD requirements. However, the relationship between the requirements and the strength and deformation capacity of H-section beams subjected to cyclic loading has not been clarified yet.

This paper discusses the cyclic loading tests conducted on H-section beam specimens with three types of supports at their top flnages, to investigate the effect of the stiffnesses of lateral and rotational supports on their strength and inelastic deformation capacity. Numerical analysis models using the finite element method were employed to simulate the inelastic behavior of the specimens and the effect of the sectional stiffener. Finally, simulations with different values of unbraced length, lateral and rotational stiffnesses, sectional stiffener mount, and dead load condition were conducted to investigate the relationship between the beam bracing requirements and their strength and deformation capacity.

2. Beam Bracing Requirements in Japanese Provisions

Several Japanese provisions have provided beam bracing requirements for bending members, as summarized below.

2.1 *AIJ's Recommendation for LSD of Steel Structures*

The required stiffness and strength are given as

$$K = \frac{5}{l_b}\frac{M_p}{h} \tag{1}$$

$$F = 0.03\frac{M_p}{h} \tag{2}$$

$$K_B = \frac{8}{l_b}M_p h \tag{3}$$

$$M_B = 0.03\frac{M_h}{h}\tilde{h} \tag{4}$$

where K (Fig. 1) and F are the required stiffness and strength, respectively, of the lateral bracing support, K_B (Fig. 1) and M_B are the required stiffness and strength, respectively, of the rotational bracing support, M_p is the plastic moment, h is the depth of the beam, and $\tilde{h}$ is the length between the points of the supports and the compression flange.

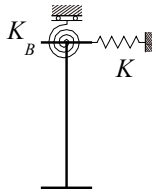

Figure 1: Lateral and rotational stiffnesses of supports

Table 1: Classification of beam slenderness in LSD

L-I	L-II	L-III
$\lambda_b \le 0.75\ {}_p\lambda_b$	$0.75\ {}_p\lambda_b < \lambda_b \le {}_p\lambda_b$	$\lambda_b < {}_p\lambda_b$

The slenderness ratio λ_b is given as

$$\lambda_b = \sqrt{\frac{M_p}{M_e}} \tag{5}$$

where M_e is the elastic lateral-torsional buckling strength.
The plastic limiting slenderness ratio ${}_p\lambda_b$ is given as

$${}_p\lambda_b = 0.6 + 0.3\left(\frac{M_2}{M_1}\right) \tag{6}$$

where M_1 and M_2 are the smaller and larger moments, respectively, at the end of the unbraced length of the support. The value of M_2/M_1 is positive when the moments cause reverse curvature. The slenderness ratio of the beams is classified into three types, as listed in Table 1.

2.2 *AIJ's Recommendation for the Plastic Design (PD) of Steel Structures*
The required unbraced length for SN400 and SS400 steel specified by the Japanese Industrial Standard is given as

$$\begin{cases} -1.0 \le \dfrac{\bar{M}}{M_p} \le 0.5 & \dfrac{l_b \cdot h}{A_f} \le 250 \ \textit{and}\ \dfrac{l_b}{i_y} \le 65 \\ 0.5 \le \dfrac{\bar{M}}{M_p} \le 1.0 & \dfrac{l_b \cdot h}{A_f} \le 375 \ \textit{and}\ \dfrac{l_b}{i_y} \le 95 \end{cases} \tag{7}$$

where l_b is the unbraced length, $\bar{M}$ is the absolute value of the smaller moment at the end of the unbraced length, A_f is the cross-sectional area of the compression flange, and i_y is the weak axis radius of gyration of the beam.

2.3 *Structural design provision by Building Center of Japan (BCJ)*
When lateral supports are provided uniformly along the axis, the required unbraced length for SS400 steel is given as

$$\lambda_y \le 170 + 20n \tag{8}$$

where λ_y is the weak axis moment of inertia of the beam and n is the number of lateral supports. When supports are provided at the end of the beam, the required unbraced length for SS400 steel is given as

$$\frac{l_b \cdot h}{A_f} \leq 250 \; and \; \frac{l_b}{i_y} \leq 65 \tag{9}$$

3. Cyclic Loading Tests on Scaled Beam with Supports Attached to Top Flange

Cyclic loading tests were conducted to investigate the effect of the type of support (lateral or rotational) on the lateral buckling behavior of the H-section beam.

3.1 *Specimen summaries*

Fig. 2 illustrates a specimen used for cyclic loading tests. The member sizes and dimensions of the specimens were chosen to be approximately 0.2 times the large-scale framing used for actual moment frames. Each beam measured 120 × 40 × 2.3 × 3.2 mm, and column, 125 × 125 × 4.5 mm in section, across all specimens. Coupon tests for the beam and column indicated material properties as listed in Table 2. The yield strength is quite larger than the standard JIS G 3101 value for SS400 steel owing to its plate thickness. To achieve elastoplastic lateral buckling behavior, the plastic moment of the beam was maintained lower than its elastic buckling moment, as listed in Table 3. Table 4 lists the specimens and results of the requirement checks (based on the LSD and the BCJ) employing four types of specimens. As seen in Fig. 3, the specimen label was defined using both support conditions and requirement checks. The specimen labeled N-U had no bracing; L-U had only lateral support; LR-U had lateral and rotational supports but did not satisfy the bracing requirement of the LSD; and LR-S had both supports and satisfied the LSD requirement. Figs. 4 and 5 show a bar and plate made of steel, providing the lateral and rotational supports, respectively. The diameter of the steel bar was 10 mm. The thicknesses of the steel plate were 9 and 16 mm for specimens LR-U and LR-S, respectively.

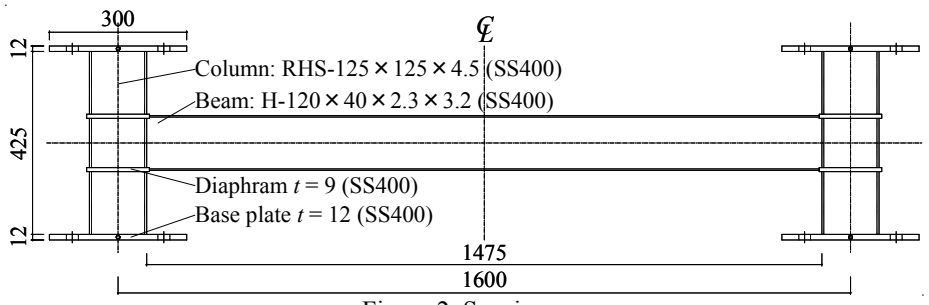

Figure 2: Specimen

Table 2: Material properties

Position	Material	Yield strength σ_y (N/mm^2)	Maximum strength σ_u (N/mm^2)	Elongation E_{long} (%)	Width-thickness ratio
Beam flange	SS400	346	458	25.7	6.3
Beam web		388	454	24.6	49.4
Column		365	438	27.8	27.8

Table 3: Beam sectional properties

Elastic lateral buckling moment M_e (kNm)	Plastic Moment M_p (kNm)	Lateral buckling slenderness ratio λ_b	Slenderness ratio λ_y
8.86	8.05	0.77	181

Table 4: Specimens and requirement checks

Specimen	Unbraced length l_b (mm)	Lateral support stiffness K_u (N/mm)	Rotational support stiffness K_β (Nmm)	Limit unbraced length (mm)	Lateral support requirement K (N/mm)	Rotational support requirement K_B (Nmm)	Check		
							Unbraced length (BCJ and LSD)	Lateral support (LSD)	Rotational support (LSD)
N-U	1475.0	0	0	737.5 (One support)	455	1.05×10^7	N.G.	N.G.	N.G.
L-U	737.5	1748					O.K.	O.K.	N.G.
LR-U	737.5		1.07×10^6				O.K.	O.K.	N.G.
LR-S	737.5		3.39×10^7				O.K.	O.K.	O.K.

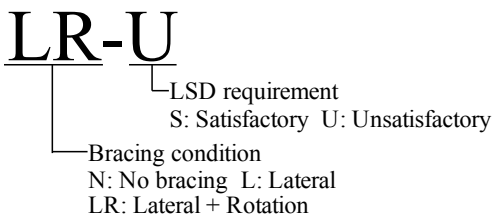

Figure 3: Specimen label

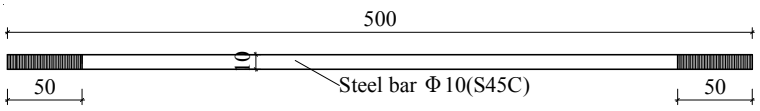

Figure 4: Lateral support

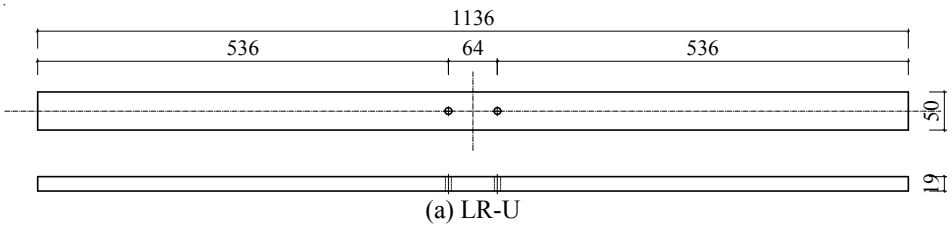

(a) LR-U

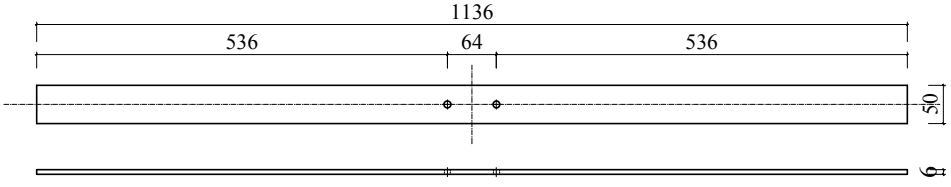

(b) LR-S

Figure 5: Rotational support

3.2 *Experimental program overview*

The specimen was fixed to the reaction beam and sliding table as shown in Fig. 6. Cyclic loading was controlled by the sliding table displacement. Fig. 7 shows the specimen modeling, which indicates that the bending moment occurs between the points of contrary flexure and that both columns were pin-ended. Fig. 8 shows the loading protocol (quasistatic). Loading was determined by the story drift. The loading continued until the 20th cycle of the 0.04 rad story drift. The test specimen was monitored with strain gauges, LVDTs, and string potentiometers, among others. The out-of-plane displacement was calibrated with a wire rope attached to a partial circular plate to eliminate torsional deformation of the section.

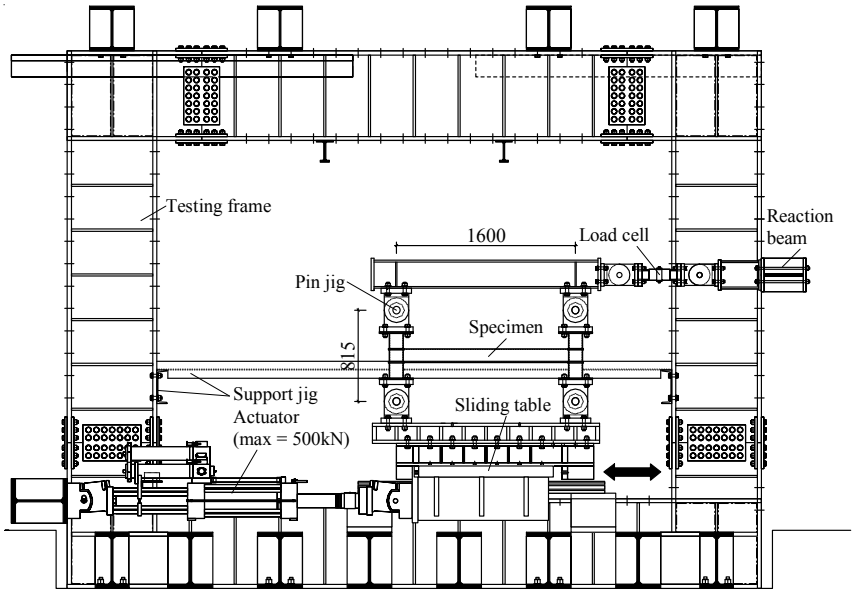

Figure 6: Test setup

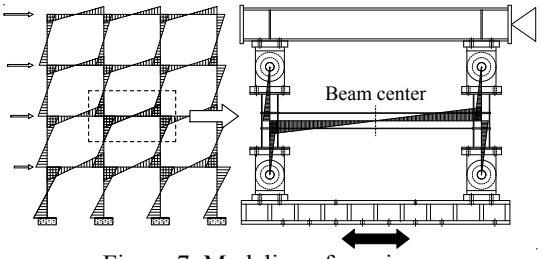

Figure 7: Modeling of specimen

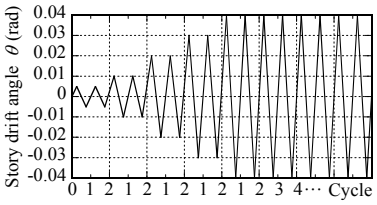

Figure 8: Loading protocol

Generally, the beam rotational angle is approximately 0.4–0.6 times the story drift. However, in this experiment, since the column stiffness was largely higher than the beam's, the beam rotational angle was assumed to be maintained equal to the story drift. The supports were attached to the midspan of the beam, as shown in Fig. 9. The steel bars were pretensioned to provide double lateral stiffness to the beam.

3.3 *Support stiffness configuration*

3.3.1 *Lateral stiffness*

The stiffness of the lateral support was determined by the steel bar and the support jig. As illustrated in Fig. 10, lateral force was applied to one of the steel bars and the lateral stiffness from the force–displacement relationship (Fig. 11) was observed twice and assessed as 873.9 N/mm, on average. The lateral stiffness of the support K_u was estimated as twice the average value (1748 N/mm), as listed in Table 4.

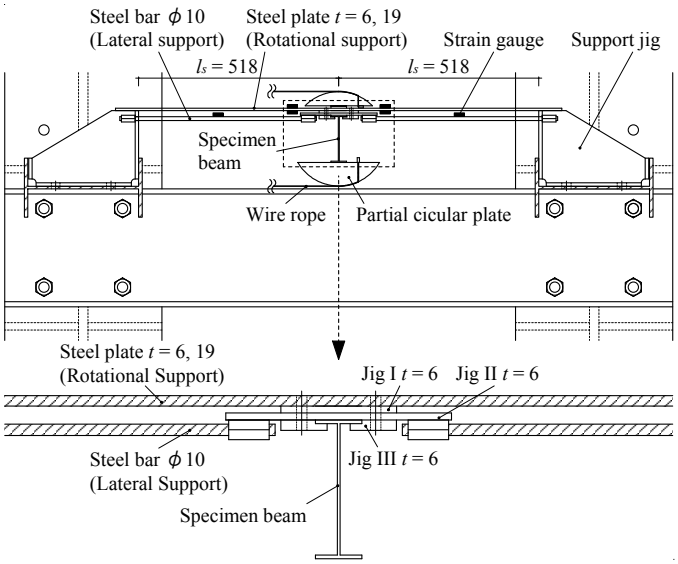

Figure 9: Lateral and rotational supports

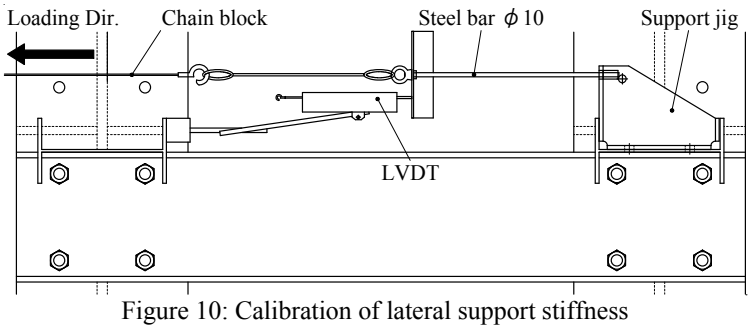

Figure 10: Calibration of lateral support stiffness

3.3.2 *Rotational stiffness*

The rotational stiffness of the support was determined by the bending stiffness of the steel plate, as given by Eq. (10).

$$K_\beta = \frac{3EI_x}{l_s} \tag{10}$$

where EI_x is the bending stiffness of the steel plate in the weak axis and l_s is the span.

3.3.3 *Comparison of stiffness with requirement*

The lateral stiffness of the L-U, LR-U, and LR-S specimens satisfied the requirement K = 455 N/mm, as shown in Table 4. The rotational stiffness of the LR-U specimen did not satisfy the requirement $K_B = 1.05\times10^7$ Nmm whereas that of the LR-S specimen did.

3.4 *Experimental results*

3.4.1 *Strength and cumulative deformation capacity*

Figure 12 shows the moment–angle response plots. Since fracture was observed at the end of the beam after the 10th cycle of the 0.04-rad story drift, the data until this are presented. The maximum strength and lateral buckling in the N-U specimen were observed at the first cycle of θ_x = +0.02 rad, when strength degradation occurred. For the L-U, LR-U, and LR-S specimens, the maximum strength and lateral buckling were observed at the first cycle of θ_x = +0.03 rad, when strength degradation was not significant compared to the N-U specimen under the 0.03-rad cycle but local buckling at the end of the beam caused gradual strength degradation. Therefore, the supports had an effect on the instant of local buckling and formation of hysteresis loops. However, the difference in the hysteresis loops in the specimens with supports (L-U, LR-U, and LR-S) was not significant. It is important to note that in case of the support satisfying the stiffness requirement in the LSD and BCJ, the ultimate strength would have possibly degraded under cyclic loading.

The moment–cumulative angle plots are shown in Fig. 13, representing the cumulative angle at 10% and 20% strength degradation ($\Sigma\theta_{x,10\%}$ and $\Sigma\theta_{x,20\%}$, respectively). For the N-U specimen, $\Sigma\theta_{x,10\%}$ and $\Sigma\theta_{x,20\%}$ were 0.07 and 0.18 rad, respectively whereas for the L-U, LR-U, and LR-S specimens, they were 0.16 and 0.27 rad, respectively, indicating an improvement in the cyclic deformation capacity.

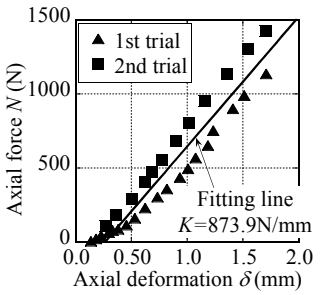

Figure 11: Lateral support force–deformation relationship

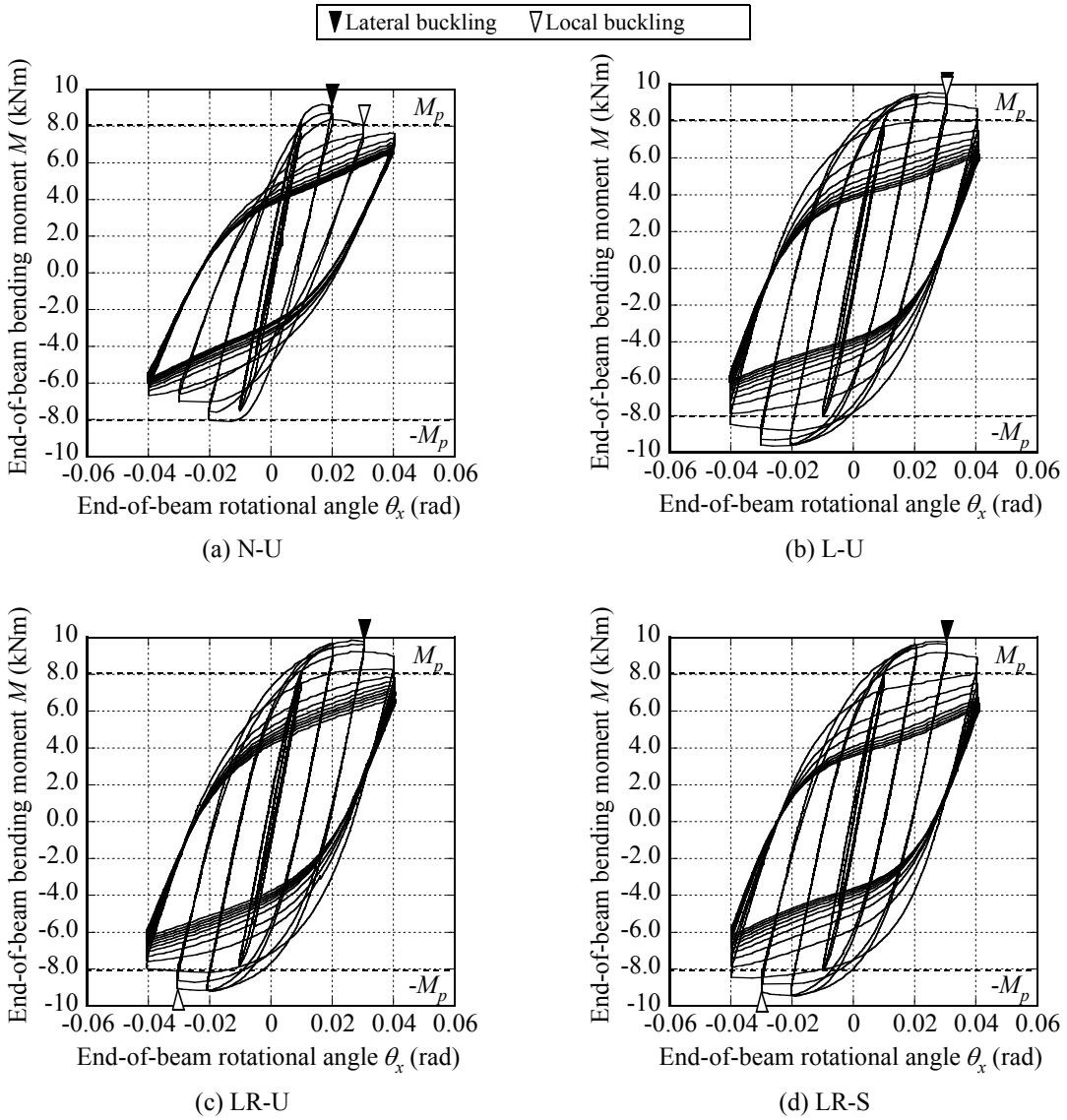

Figure 12: End-of-beam bending moment–rotational angle relationship

3.4.2 *Out-of-plane displacement transition and lateral buckling deformation of flange*

Figure 14 and Photo 1 present the out-of-plane displacement transition and deformation, respectively, of the flange. With the reversing of loading direction, the deformation of the top and bottom flanges reversed in the N-U and LR-U but occurred in the same direction in the L-U and LR-S specimens. The deformation of the top flange was restrained whereas that of the bottom flange was significant in the LR-S specimen. In the N-U specimen, the center of twist at the midspan was placed at the center of the web whereas in the LR-S specimen, web deformation was caused by the lateral deflection of the bottom flange.

Fig. 15 shows the torsional angle transition of the flange and the web (θ_z) at the supports in the LR-S specimen. The maximum value of the torsional angle of the bottom and top flanges, and the web were approximately 20° and 8°, respectively. Therefore, web deformation significantly developed in the LR-S specimen.

3.4.3 *Lateral bracing force and rotational bracing moment*

The lateral bracing force and the rotational bracing moment were calculated using the strain gauges attached to the surface of the supports, as shown in Fig. 16. Fig. 17 illustrates the transition of these two parameters, where P_y (M_p/h) is the compressive force of the flange when subjected to plastic moment M_p, and e is the eccentricity. Both force and moment in the experiments were lower than the requirements in the LSD.

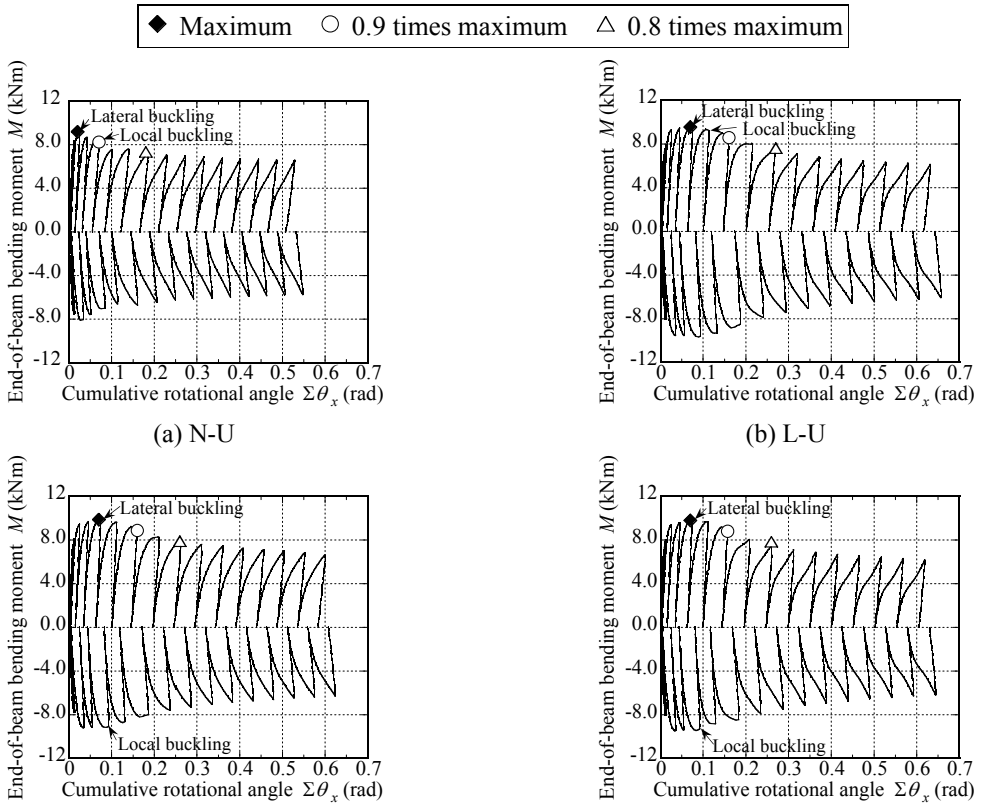

Figure 13: End-of-beam bending moment–rotational angle relationship

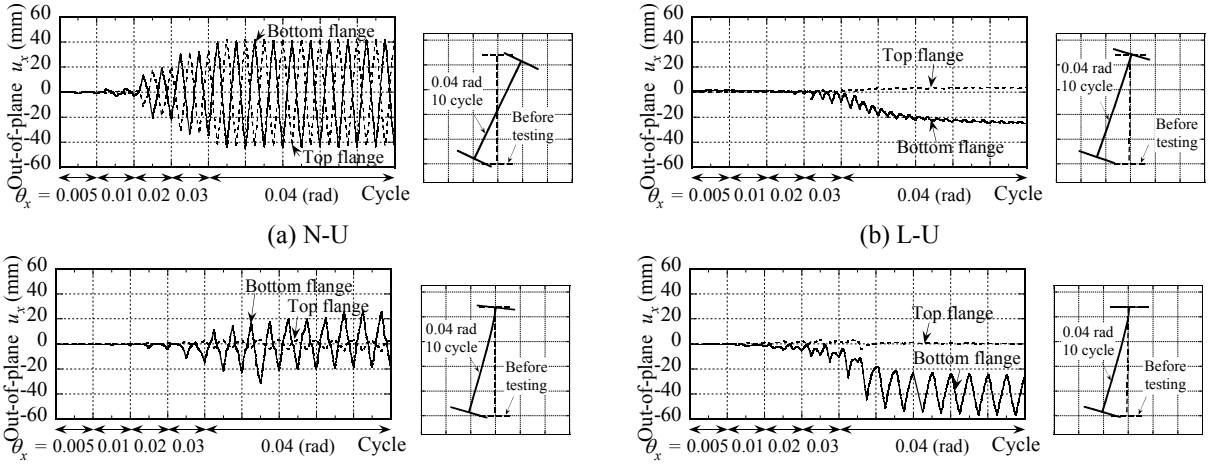

Figure 14: Out-of-plane displacement transition and sectional deformation

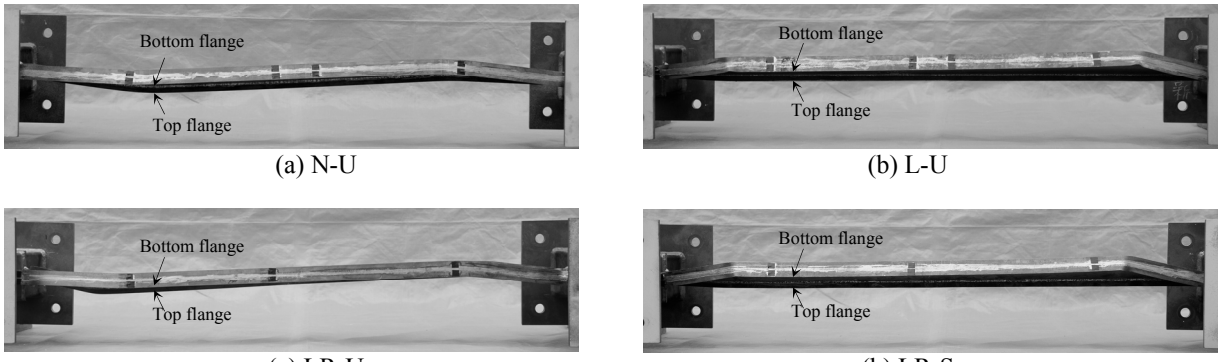

(a) N-U (b) L-U

(c) LR-U (b) LR-S

Photo 1: Specimen deformation after testing

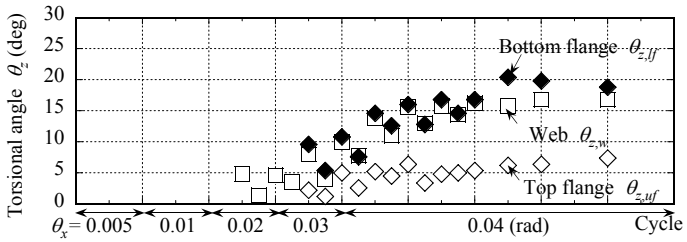

Figure 15: Torsional angle transition of flange and web

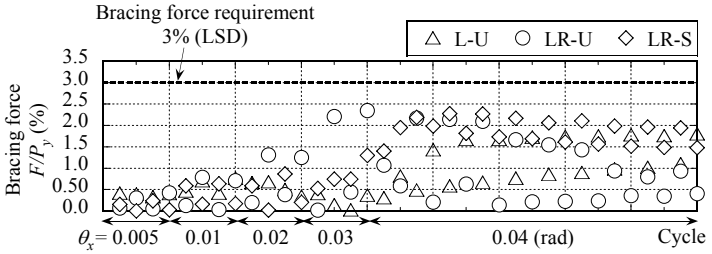

Figure 16: Bracing force transition

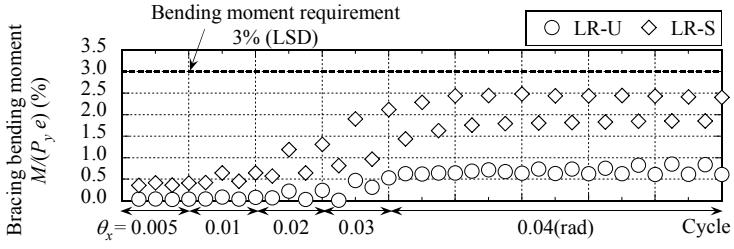

Figure 17: Bracing moment transition

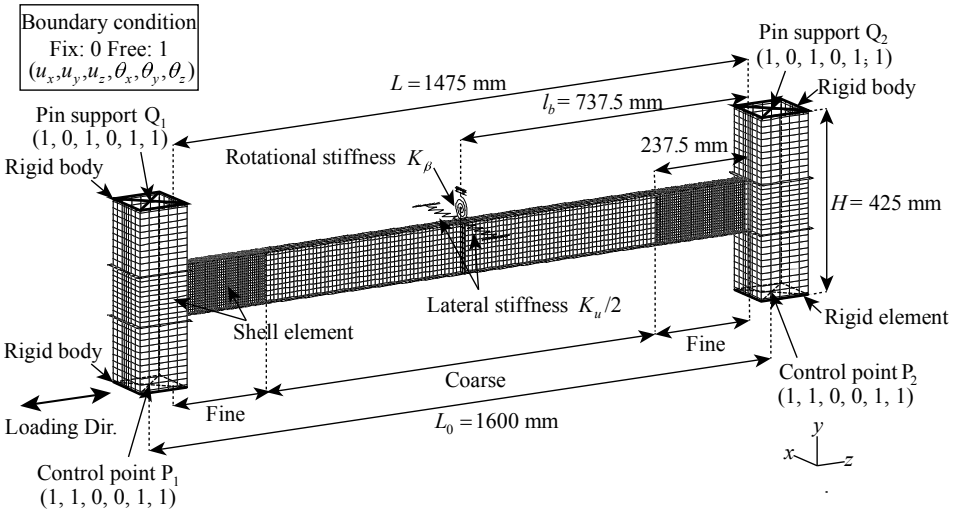

Figure 18: Numerical simulation model

4. Analytical Investigation of Cyclic Loading Tests

In this section, the experiments were simulated numerically using ABAQUS Standard ver. 6.8–11 to investigate the elastoplastic lateral buckling behavior. Additionally, the effect of a sectional stiffener at the support position was also investigated.

4.1 *Analytical model summary*

Fig. 18 shows the finite element model of the specimen, illustrating the fine mesh in the local buckling region. An additional model (labeled LR-S_s) was developed with a sectional stiffener (of thickness 2.3 mm) mounted at the support position. The shape of the global imperfection was based on the half sine wave of the beam and its amplitude was 0.001 times the global length. The numerical simulation employed shell elements, with the column and beam elements being elastic and elastoplastic, respectively. The von Mises yield surface and a combination of isotropic and kinematic hardening were employed to simulate the cyclic inelastic plasticity. The multiaxial plasticity model was calibrated based on a uniaxial tensile coupon test, and the Young's modulus and Poisson's ratio were 205,000 N/mm^2 and 0.3, respectively. Additionally, residual stress was employed to the beam shell element.

4.2 *Simulation results*

Figs. 19 (a)–(c) compare the experimental moment–angle response from Section 3.4.1 with the simulation results and indicate consistency between both results, with strength degradation occurring after the 0.03-rad cycle. The results thus confirmed the validity of the numerical simulations. For the LR-S_s specimen, the moment–angle response was stable and pinching effect was not observed, as seen from Fig. 19 (d). As illustrated in Fig. 20, this specimen shows no lateral deflection of the section at midspan and achievement of adequate bracing.

Figs. 21 and 22 show the lateral bracing force and the rotational bracing moment obtained from numerical simulation. In some cases, the former was larger than the LSD requirement. This numerical result is different from the experiment (as seen from Fig. 16) because the experimental data were not adequate to precisely assess the lateral bracing force as the strain gauge was attached to only one side of the specimen surface.

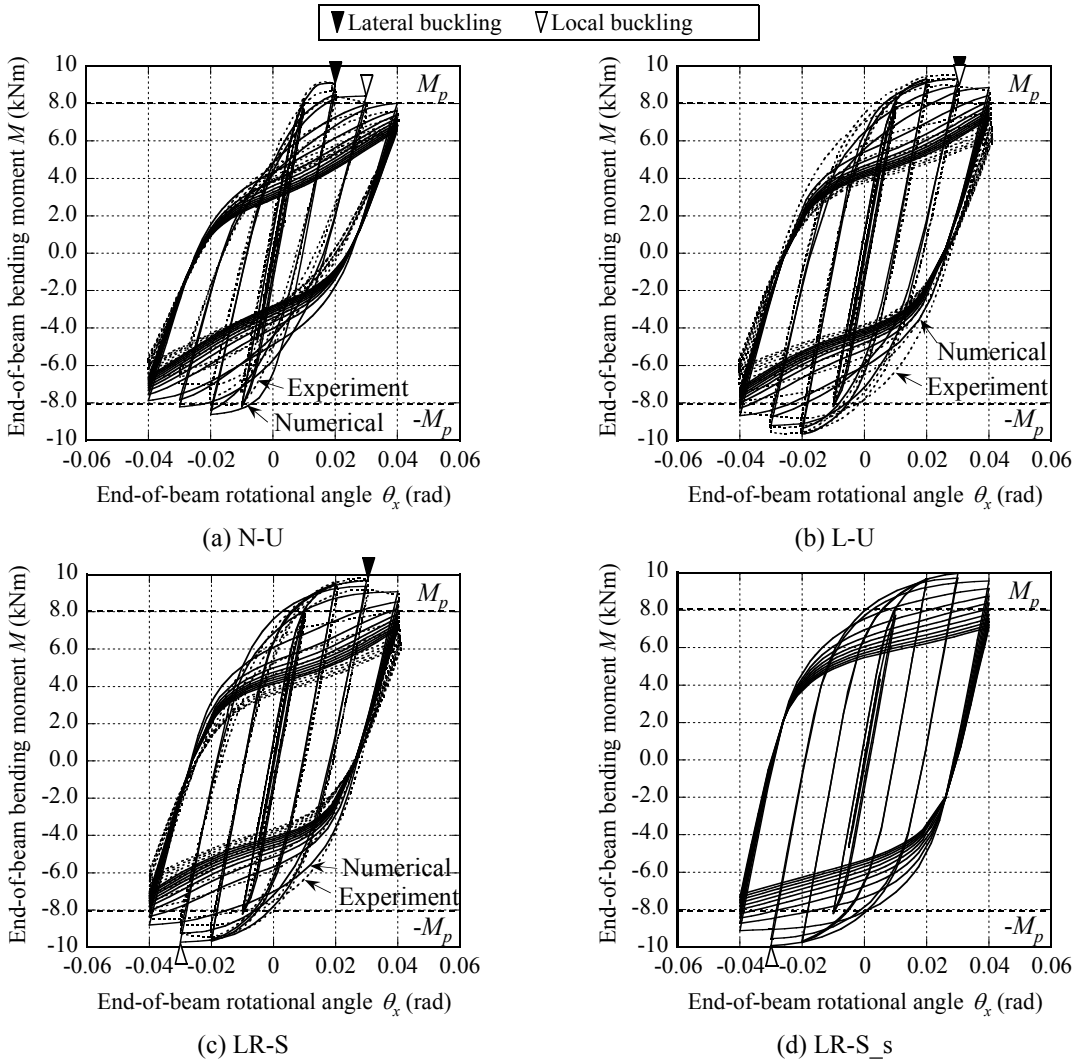

Figure 19: End-of-beam bending moment–rotational angle relationship

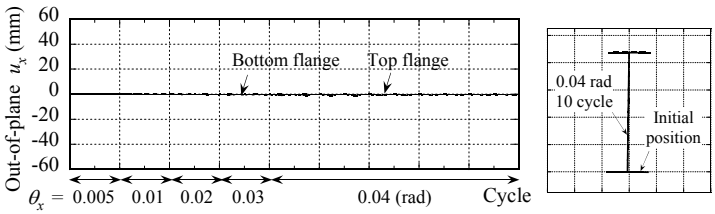

Figure 20: Out-of-plane displacement transition and sectional deformation (LR-S_s)

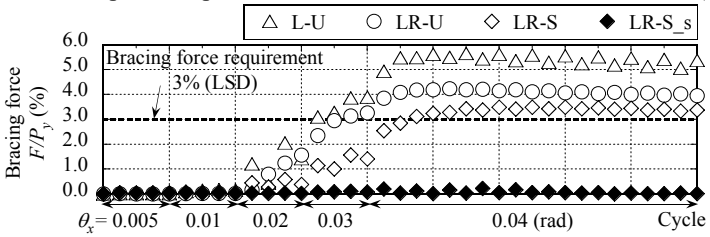

Figure 21: Bracing force transition (numerical simulation)

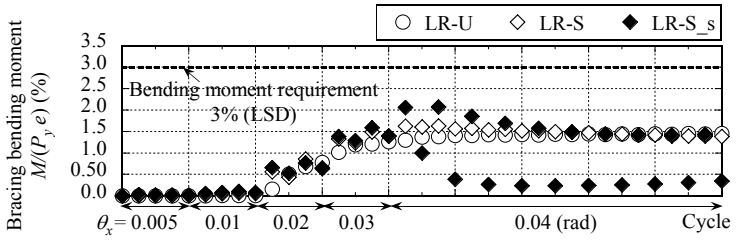

Figure 22: Bracing bending moment transition (numerical simulation)

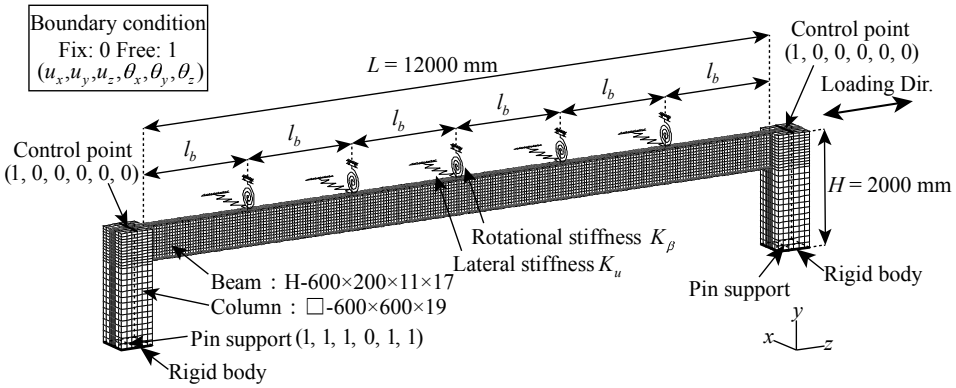

Figure 23: Numerical simulation model

5. Assessment of Lateral and Rotational Supports under Cyclic Loading

The finite element method was used for assessing the bracing condition of the H-section beams. The numerical model illustrated in Fig. 23 was used for modeling the one-span moment frame. The beam and column sections measured H-600×200×11×17 and □-600×600×19, respectively. Their lengths were, respectively, 12.0 and 2.0 m, considering the distance between the points of contrary flexure. Models with varying unbraced length, lateral and rotational stiffnesses, sectional stiffener mount, and dead load condition were developed, the conditions for which are summarized in Table 5. The dead and live loads were set to 4.2 and 1.8 kN/m^2, respectively, based on the regular office building and the total load of 6.0 kN/m^2 was introduced to each node uniformly. The multiaxial plasticity model was calibrated based on the uniaxial tensile coupon test conducted by Takeuchi et al. (2010) as shown in Fig. 24. The initial imperfection was provided as in Section 4. To identify the capacity of the cumulative dissipation energy (CDE), an index χ was introduced as given by Eqs. (11)–(13).

$$\chi = \frac{W}{M_p \theta_p} = \frac{\int M d\theta}{M_p \theta_p} \tag{11}$$

$$\theta_p = \frac{M_p L}{6EI_x} \tag{12}$$

$$M_p = \sigma_y Z \tag{13}$$

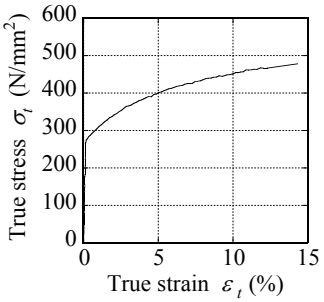

Figure 24: Inelastic material property

Table 5: Numerical simulation model parameters

Section	H-600×200×11×17
Beam length L (m)	12.0
Unbraced length l_b (m)	0.2/0.5/1.0/2.0/3.0/6.0/12.0
Lateral stiffness K_u/K	0.0/0.5/1.0/2.0
Rotational stiffness K_β/K_B	0.0/0.5/1.0/2.0
Stiffener	Mounted/Not mounted
Dead load	Considered/Not considered

Table 6: Beam sectional properties

Yield stress σ_y (N/mm^2)	235
Plastic modulus Z (mm^3)	2.89×10^6
Moment of inertia of strong axis I_x (mm^4)	7.44×10^8
Plastic moment M_p (kNm)	679
Yield Rotational angle θ_p (rad)	0.0089

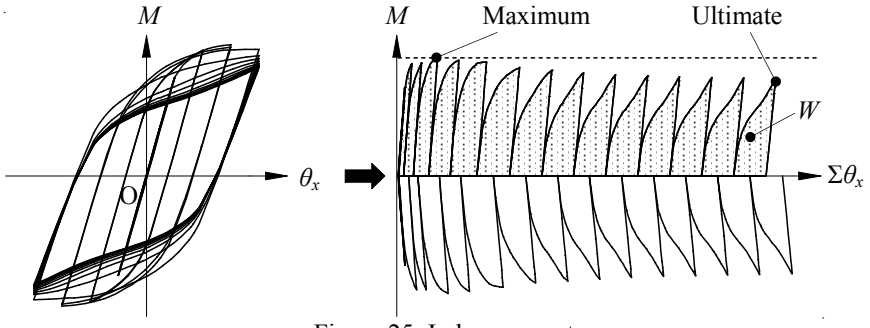

Figure 25: Index concept

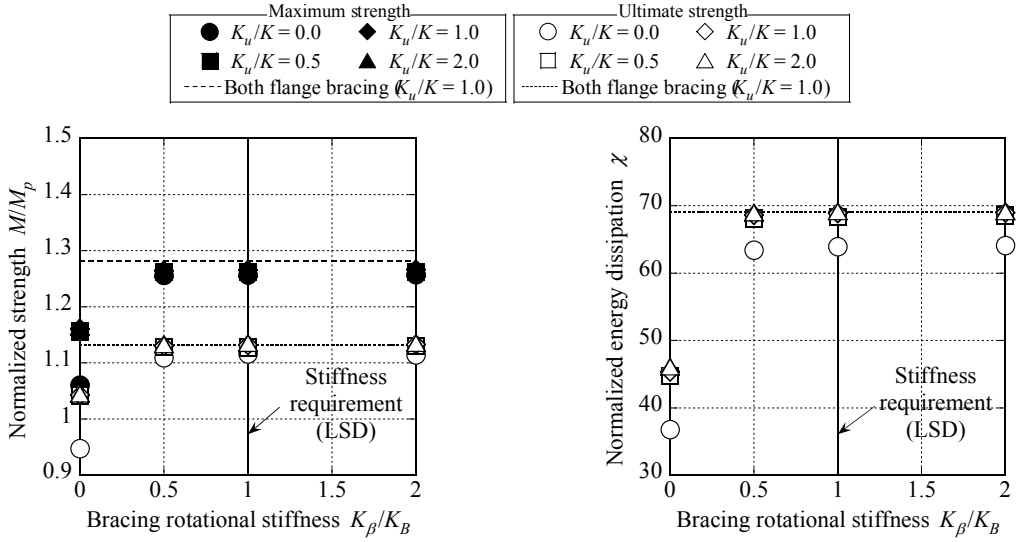

(a) Normalized strength (b) Normalized energy dissipation

Figure 26: Influence of support stiffness (l_b = 2000 mm)

where W is the CDE on the positive side until the 10th 0.04-rad cycle, M_p is the plastic moment, θ_p is the angle occurring when M_p is reached based on the elastic modulus, L is the beam length, σ_y is the yield stress, and Z is the plastic modulus. The concept of the CDE is illustrated in Fig. 25 and the beam dimensions are summarized in Table 6.

5.1 *Effect of lateral and rotational support stiffnesses*

Fig. 26 shows the strength–rotational stiffness and CDE–rotational stiffness relationships when the unbraced length l_b was 2000 mm, the sectional stiffener was not mounted, and the dead load was not considered. The dotted line represents the results when both top and bottom flanges were braced (both-flanges-braced model).

When the lateral stiffness K_u/K and the rotational stiffness K_β/K_B were equal to 1.0, adequate bracing was available to prevent lateral buckling, and the strength and CDE were approximately equivalent to those of the both-flanges-braced model (i.e., the strength and CDE of the model with $K_u/K = K_\beta/K_B = 0.5$ were largely equivalent to that with $K_u/K = K_\beta/K_B = 1.0$), thus confirming that the LSD recommendation leads to a safer design. In contrast, the strength and CDE of the model with $K_u/K = K_\beta/K_B = 2.0$ were not significantly different from that with $K_u/K = K_\beta/K_B = 1.0$ because the two parameters were determined by local buckling when adequate bracing was provided.

5.2 *Effect of unbraced length*

Fig. 27 shows the strength–rotational stiffness and CDE–rotational stiffness relationships at l_b = 2000 mm and $K_u/K = 1$, and when the sectional stiffener was not mounted and the dead load not considered. As the rotational stiffness increased, the strength and CDE asymptotically reached certain values and hence, the bracing requirements in the LSD ensured that adequate bracing under cyclic loading was provided. As the unbraced length decreased, the strength and CDE performances improved.

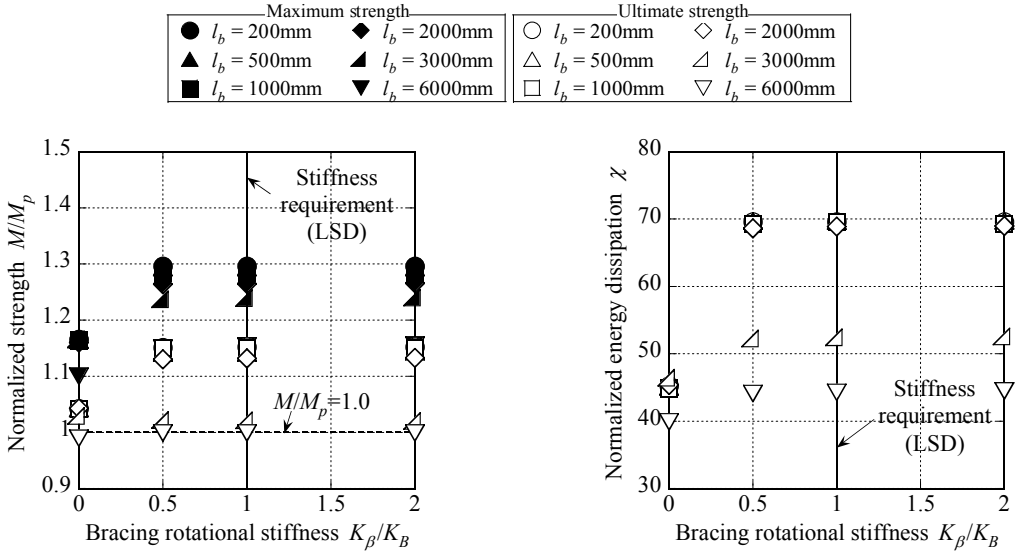

(a) Normalized strength (b) Normalized energy dissipation

Figure 27: Influence of unbraced length (K_u/K = 1.0)

5.3 *Effect of sectional stiffener at supports and dead load*

Fig. 28 shows the strength–rotational stiffness and CDE–rotational stiffness relationships for l_b = 2000 mm, and $K_u/K = K_\beta/K = 1$. The unbraced length requirements given by each provision are also illustrated.

When the sectional stiffener was not mounted, the difference between the CDE values of models was not significant when l_b was <2000 mm, which satisfied the bracing requirement of the PD, BCJ, and LSD in the L-I category. However, when l_b was 3000 mm, satisfying only the LSD requirements in the L-II category, the CDE was smaller than that of other models. The sectional stiffener did not affect the CDE for l_b < 2000 mm but did for l_b = 3000 mm. Similarly, the dead load affected the strength and CDE of the model for l_b = 3000 mm but did not affect the difference between the two parameters.

5.4 *General summary*

The general summary of Section 5 is given below, followed by the results of the numerical simulation of various model parameters.

The strength and CDE of the beam with adequate lateral and rotational supports at the top flange and satisfying the bracing requirement of the LSD were approximately equivalent to those of the beam with adequate lateral supports at both top and bottom flanges under cyclic loading. The lateral and rotational supports with high stiffnesses did not necessarily impart higher strength to the beam because strength was determined by local buckling when the two supports at the top flange satisfied the bracing requirement of the LSD.

Under cyclic loading, the sectional stiffener and dead load affected the strength but not the CDE when l_b satisfied the bracing requirement of the PD, BCJ, and LSD in the L-I category, but affected both the strength and CDE when l_b satisfied only the bracing requirement of the LSD in the L-II category. Generally, the current Japanese provisions were valid for the assessment of beam bracing.

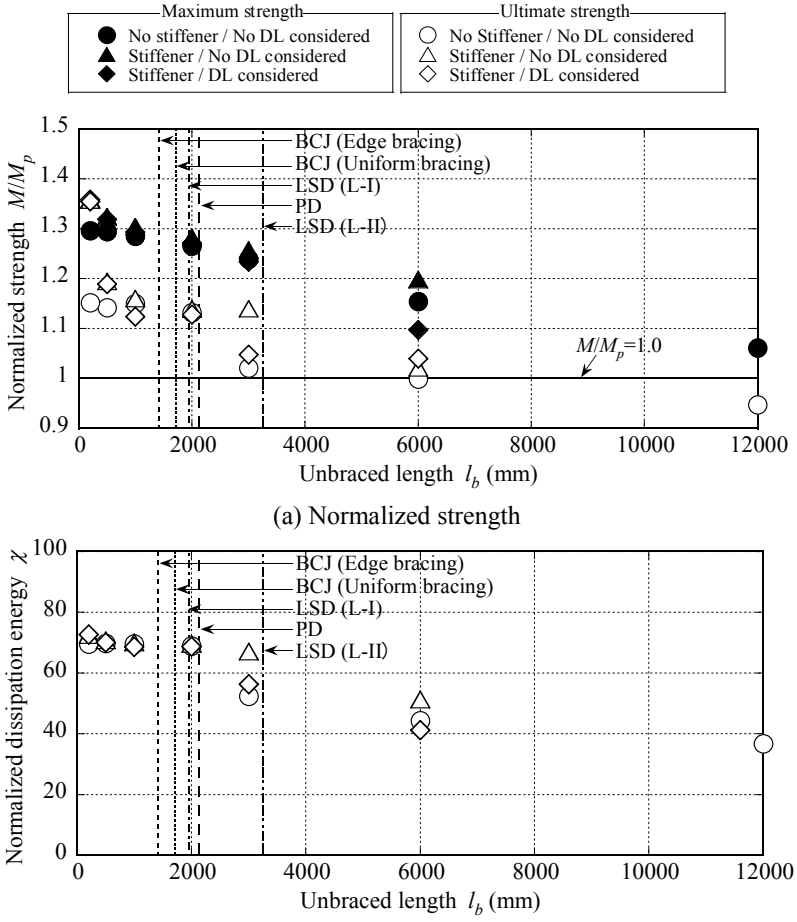

(a) Normalized strength

(b) Normalized energy dissipation

Figure 28: Influence of unbraced length ($K_u/K = K_\beta/K = 1.0$)

6. Conclusions

This paper presents the test of validity of the bracing requirements for the top flange of H-section beams given by the current building provisions subjected to cyclic loading. Experiments and numerical simulations were conducted to assess the effect of unbraced length, lateral and rotational stiffnesses of the bracing supports, sectional stiffener mount, and dead load condition on the strength and cumulative deformation energy of beams under cyclic loading. From the studies, the following conclusions were drawn:

1. When beams possess ductile deformation capacity under monotonic loading, strength degradation possibly occurs under cyclic loading in those beams with adequate lateral and rotational support at the top flange.
2. When a sectional stiffener is mounted at the bracing support position, the top flange bracing requirement given by the current Japanese provisions is viable to impart strength and cumulative energy dissipation to the beam with adequate bracing at both top and bottom flanges.

3. When the lateral and rotational supports at the top flange satisfy the current Japanese provisions, their high stiffness does not necessarily impart higher strength to the beam because strength is determined by local buckling.
4. When the unbraced length satisfies the requirement given by most of the current Japanese provisions, the sectional stiffener and dead load affect the strength but not the cumulative deformation energy. However when it satisfies the bracing requirement of Limit Design Standard of Steel Structures of Architectural Institute of Japan in the L-II category, they affect both strength and cumulative dissipation energy.

Acknowledgments

A part of this research was supported by Grants-in-Aid for Scientific Research of the Japan Society for the Promotion of Science (Research Project Number: 24760448).

References

American Institute of Steel Construction. (2010). "Specification for Structural Steel Buildings."

Ando, S. and Ono, T. (2005). "Buckling strength and deformation capacity of bracing beam considering local and lateral buckling." *Summaries of technical papers of Annual Meeting Architectural Institute of Japan. C-1, Structures III, Timber structures steel structures steel reinforced concrete structures,* Architectural Institute of Japan, 695-696

Architectural Institute of Japan. (2005). "Design Standard for Steel Structures -Based on Allowable Stress Concept-." (in Japanese).

Architectural Institute of Japan. (2009). "Recommendations for Stability Design of Steel Structures." (in Japanese).

Architectural Institute of Japan. (2010). "Recommendation for Limit State Design of Steel Structures." (in Japanese).

Architectural Institute of Japan. (2010). "Recommendation for the Plastic Design of Steel Structures." (in Japanese).

Galambos, T. V. (1963). "Inelastic lateral buckling of beams." *Journal of Structural Division*, ASCE, 89 ST. 5

Nakashima, M., Kanao, I. and Liu, D. (2002). "Lateral instability and lateral bracing of steel beams subjected to cyclic loading." *Journal of Structural Engineering,* ASCE, 128 (10) 1308-1316.

Liu, D., Nakashima, M. and Kanao, I. (2003). "Behavior to complete failure of steel beams subjected to cyclic loading." *Journal of Engineering Structures,* Elsevier, 25 (5) 525-535.

Takeuchi, T., Hajjar, J. F., Matsui, R., Nishimoto, K. and Aiken, I. D. (2010). "Local buckling restraint condition for core plates in buckling restrained braces." *Journal of Constructional Steel Research,* Elsevier, 66 (2) 139-149.

Wakabayashi, M. and Nakamura, T. (1983). "Buckling of laterally braced beams." *Journal of Engineering Structures,* Elsevier, 5 (2) 108-118.